

Complexity of localised coherent structures in a boundary-layer flow

Taras Khapko^{1,2}, Johann Duguet³, Tobias Kreilos^{4,5}, Philipp Schlatter^{1,2}, Bruno Eckhardt^{4,6}, and Dan S. Henningson^{1,2}

¹Linné FLOW Centre, KTH Mechanics, Osquars Backe 18, SE-100 44 Stockholm, Sweden

²Swedish e-Science Research Centre (SeRC)

³LIMSI-CNRS, UPR 3251, F-91403 Orsay Cedex, France

⁴Fachbereich Physik, Philipps-Universität Marburg, Renthof 6, D-35032 Marburg, Germany

⁵Max Planck Institute for Dynamics and Self-Organization, Am Fassberg 17, D-37077 Göttingen, Germany

⁶J.M. Burgerscentrum, Delft University of Technology, Mekelweg 2, NL-2628 CD Delft, The Netherlands

June 17, 2021

Abstract

We study numerically transitional coherent structures in a boundary-layer flow with homogeneous suction at the wall (the so-called asymptotic suction boundary layer ASBL). The dynamics restricted to the laminar–turbulent separatrix is investigated in a spanwise-extended domain that allows for robust localisation of all edge states. We work at fixed Reynolds number and study the edge states as a function of the streamwise period. We demonstrate the complex spatio–temporal dynamics of these localised states, which exhibits multistability and undergoes complex bifurcations leading from periodic to chaotic regimes. It is argued that in all regimes the dynamics restricted to the edge is essentially low-dimensional and non-extensive.

1 Introduction

Understanding how boundary-layer flows become turbulent is of crucial importance for many applications, in particular for all aeronautic purposes, because of the increased drag associated with turbulent fluctuations. Since in most applications drag needs to be kept as low as possible, control strategies aim at delaying the transition from laminar to turbulent. The problem of transition to turbulence has long been addressed using linear stability theory, where typically one looks for a critical value of a governing parameter above which the laminar base flow loses its stability with respect to infinitesimal disturbances. For instance, in the case of the incompressible flat plate Blasius boundary-layer flow, a Reynolds number $Re = U_\infty \delta / \nu$ can be constructed using the free-stream velocity U_∞ , the local displacement thickness δ at the given streamwise location, and the kinematic viscosity ν of the fluid. The critical value of Re given by linear stability theory is $Re_c \approx 520$, which corresponds to an exponential amplification of Tollmien–Schlichting (TS) waves [1]. TS waves are “connected” to the base flow, meaning that there is a continuous path in parameter space linking them to the laminar state. TS waves can actually be triggered at lower (subcritical) Re , resulting in a finite-amplitude instability of the base flow to such waves. The “classical” transition route, typical of weakly disturbed environments, corre-

sponds to the sequence of secondary bifurcations undergone by these waves [2]. Still according to linear stability theory, a control strategy that would shift the linear stability threshold would be considered efficient. We consider here the case of an incompressible boundary-layer flow stabilised by homogeneous suction at the wall. Suction counteracts the spatial development of the boundary layer, leading asymptotically to a steady laminar base flow independent of the planar coordinates, called Asymptotic Suction Boundary-Layer flow (ASBL) [3], see fig. 1. Since suction shifts the linear stability threshold to 54,370 [4] it would qualify as an efficient control. However, in this flow as well as in other shear flows, a second, nonlinear path to turbulence, so-called bypass transition, can interfere with this control strategy. In the presence of stronger background fluctuations (noise, incoming turbulence, localised forcing, *etc.*), a drastically different, fully nonlinear picture emerges for transition, termed “bypass route to turbulence”. Schematically, additional solutions of the governing equations that are *not* connected to the base flow appear at a finite value of $Re = Re_{SN}$ through a saddle-node bifurcation [5, 6]. The upper branch corresponds to solutions with larger drag, representative of a stable turbulent regime. Its counterpart, the lower branch, corresponds to an unstable separatrix dividing the phase space into two basins of attraction for the laminar and turbulent

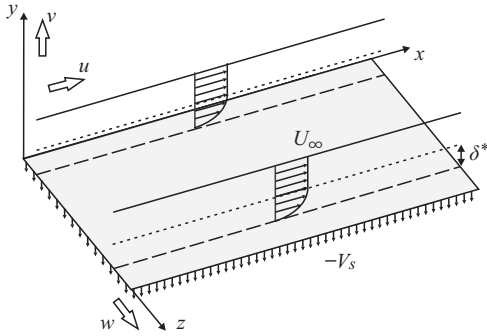


Figure 1: Sketch of the asymptotic suction boundary layer.

state, respectively. The value of Re_{SN} cannot be predicted by linear stability theory, and generally $Re_{SN} < Re_c$. Perhaps more importantly, control strategies based on linear theory also fail at predicting whether Re_{SN} is affected at all by the control, see fig. 2. There is recent evidence that Re_{SN} for both Blasius and ASBL flows is as low as 300 [7]. This points out the need for a nonlinear description of transition processes extended to controlled boundary-layer flows.

The existence of a lower branch not connected to the base flow is typical of a wider class of transition scenarios classified as “subcritical transition”, common to many wall bounded flows such as circular pipe flow, square duct flow, plane Couette flow, plane channel flow, see for instance [6, 8]. As mentioned before, the phase space is split into two regions, one where trajectories immediately return to the laminar fixed point, the other where the turbulent state is reached. Detailed investigations of the dynamics along the associated separatrix have become popular in the last decade owing to the concept of “edge state” and “edge manifold” [9]. The edge manifold (or simply “edge”) is not only the geometrical separatrix in phase space, but also an invariant subspace for the flow. Within this invariant manifold there are attractors, so-called edge states. In the simplest case, the edge state is unique and corresponds to a simple unstable solution of the system, such as a fixed point or a limit cycle, and its stable manifold (the edge) separates two attractors in state space: the laminar state and the turbulent state. For initial conditions close enough to the edge, trajectories will then approach the neighbourhood of the edge state and later leave towards one of the two attractors depending on which “side” of the edge the initial condition lies. An efficient and intrinsically nonlinear control strategy should then consist of targeting the edge state in order to shift the dynamics from the turbulent side of the edge to the laminar one [10].

When the system is not geometrically restricted by periodic boundary conditions, the edge state corresponds to a coherent structure of the flow that is always spatially localised [11, 12, 13, 14, 15]. Families of localised structures in plane Couette flow have been connected to the snaking

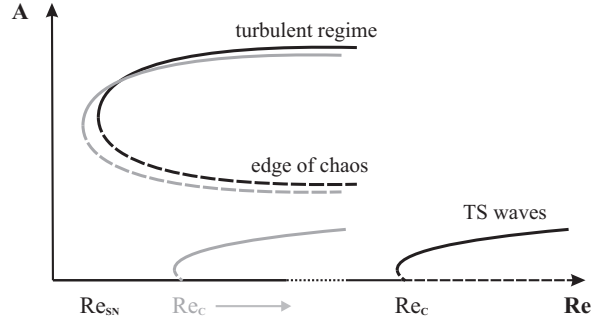


Figure 2: Schematic bifurcation diagram for the uncontrolled (grey) and controlled (black) boundary layer.

bifurcation scenarios [16, 17, 18].

Several difficulties arise, making this picture often incomplete. The first one, typical of low values of Re , occurs when the turbulent state is a chaotic saddle rather than an attractor. The stable manifold of the edge state is in that case entangled with the turbulent dynamics in a complex way, a manifestation being a finite probability of relaminarising for almost any turbulent trajectory. Such behaviour is in general linked to a boundary crisis occurring at some value of Re slightly above Re_{SN} [19, 20, 21] involving the stable manifold of the edge state. At higher Re , sudden relaminarization events are no longer observed in practice, either because turbulent lifetimes are too long on average, or because spatial proliferation of turbulent fluctuations makes the local probability for relaminarization only weakly relevant [22, 23]. Another difficulty, which we will address here, is related to simple general questions such as: “what is the expected nature of the edge state?”, “can it be chaotic?”, “is the edge state unique?” and “is it robust to changes in the parameters?”. Some of these questions have been addressed using a simple low-dimensional phenomenological model in ref. [24]. The concept of edge state as a relative attractor is an asymptotic concept only. As edge-tracking algorithms are iterative by nature, numerical evidence for chaotic edge states is hard to justify since any erratic edge trajectory is always potentially a transient approach to a more simple invariant state. Chaotic edge states have been nevertheless reported several times in the literature [25, 12, 13] and are likely to be typical if not generic in extended domains. Phase-space coexistence of different (*i.e.* not symmetry-related) edge states has been reported too [26, 27]. These questions are important from a fundamental point of view because the separatrix forms part of the skeleton of the phase space. They are also crucial from a practical point of view, a multitude of edge states calling for a non-trivial generalisation of the nonlinear control strategy suggested in ref. [10]. Apart from transition processes, studying coherent structures on the edge can also teach us about the dynamics of near-wall turbulence [28].

Recent numerical studies have focused on edge states in various models of boundary-layer flows [29, 15, 30], in particular in the case of ASBL [31, 27]. We here continue to explore the rich dynamics of edge states in the ASBL as a prototype for controlled boundary-layer flows. Following the strategy adopted in Couette flow [13], as the next step after studying small boxes [31] and prior to considering large ones, we perform numerical simulations in a periodic domain that is wide enough to display spatial localisation in the spanwise direction. Let us denote by L_x the streamwise length of the domain, which in case of periodic boundary conditions defines the fundamental streamwise wavenumber in a given computational domain. Unlike more classical procedures where the governing parameter varied is Re , here we keep the value of Re constant and consider the streamwise wavelength L_x as a varying parameter. Various types of dynamics on the edge emerge from this numerical exploration, among them period doubling, multistability and Pomeau–Manneville intermittency that are surprisingly reminiscent of many simpler systems such as coupled logistic maps [32].

The paper is structured as follows. In sect. 2 we introduce the essential features of the ASBL and recall the numerical methods combined together to identify edge states. Sect. 3 begins with examples of the low- Re dynamics of the flow and the evidence for a chaotic saddle related to the stable manifold of the edge state. The various states identified in Khapko *et al.* 2013 [27] are then tracked in parameter space *vs.* changes in L_x . Sect. 4 is devoted to a discussion of the results and suggests a more general picture of the dynamics on the basin separatrix. Finally the relevance of such localised states for the study of the turbulent regime will be discussed.

2 Flow case and numerical methods

The asymptotic suction boundary layer (ASBL) is a zero-pressure-gradient boundary-layer flow above a flat plate at which constant homogeneous suction is applied. The flow is governed by the incompressible Navier–Stokes equations

$$\frac{\partial \tilde{\mathbf{u}}}{\partial \tilde{t}} + (\tilde{\mathbf{u}} \cdot \tilde{\nabla}) \tilde{\mathbf{u}} = -\frac{1}{\rho} \tilde{\nabla} \tilde{p} + \nu \tilde{\nabla}^2 \tilde{\mathbf{u}}, \quad (1)$$

together with the continuity equation

$$\tilde{\nabla} \cdot \tilde{\mathbf{u}} = 0. \quad (2)$$

Here $\tilde{\mathbf{u}} = (\tilde{u}, \tilde{v}, \tilde{w})$ is the velocity field of the flow in the streamwise \tilde{x} , wall-normal \tilde{y} and spanwise \tilde{z} directions, respectively, \tilde{p} stands for the pressure, ρ for the fluid density and ν for the kinematic viscosity. The corresponding boundary conditions are

$$(\tilde{u}, \tilde{v}, \tilde{w})_{\tilde{y}=0} = (0, -V_S, 0), \quad (3a)$$

$$(\tilde{u}, \tilde{v}, \tilde{w})_{\tilde{y}=\infty} = (U_\infty, -V_S, 0), \quad (3b)$$

where U_∞ and V_S are the fixed free-stream and suction velocities.

The system admits a steady laminar solution with constant boundary-layer thickness,

$$(\tilde{U}, \tilde{V}, \tilde{W}) = (U_\infty(1 - e^{-\tilde{y}V_S/\nu}), -V_S, 0), \quad (4a)$$

$$\tilde{p} = \text{const}. \quad (4b)$$

The Reynolds number $Re = U_\infty \delta^* / \nu$ is based on the laminar displacement thickness

$$\delta^* = \int_0^\infty (1 - \tilde{u}(\tilde{y})/U_\infty) d\tilde{y}, \quad (5)$$

which in this case is given analytically by $\delta^* = \nu/V_S$. Accordingly, the Reynolds number is given by the ratio of the free-stream velocity and the suction velocity, $Re = U_\infty/V_S$. The free-stream velocity U_∞ and the boundary-layer thickness δ^* are used as characteristic units for the non-dimensionalisation, and we write non-dimensional quantities without tilde.

For the current study direct numerical simulations of ASBL are performed using a fully spectral code in a channel geometry [33] of finite wall-normal extent $[0, L_y]$. The details of the numerical method are discussed in ref. [27]. Whereas the streamwise extent L_x of the computational domain is varied between 4π and 6π (in units of δ^*), the height L_y and the width L_z are held constant, as well as the Reynolds number which is set to $Re = 500$ except when indicated. As shown in ref. [27], $L_y = 15$ and $L_z = 50$ are sufficient to accurately catch the localisation properties of the edge states. A resolution of $N_x \times N_y \times N_z = 48 \times 129 \times 192$ spectral modes was found suitable for the investigation of edge states within this numerical domain, resulting in a system with $N = 4N_x N_y N_z \approx 4.8 \times 10^6$ degrees of freedom for the velocities and pressure.

In order to track the dynamics on the laminar–turbulent separatrix, a bisection is performed along the line joining an arbitrary initial condition to the laminar state [9]. Each individual trajectory is followed until it approaches either the turbulent or the laminar one. Such approaches are detected using predetermined thresholds for the quantity v_{rms} , which represents root-mean-square of the wall-normal velocity fluctuations. This iterative procedure results in a trajectory that shadows the laminar–turbulent boundary for arbitrary long times. By iterating for a sufficiently long time we can determine the nature of the relative attractor on the edge, *i.e.* the edge state.

3 Results

3.1 Low- Re transient turbulence

We begin with a short description of the turbulent state obtained by numerical simulation. Our investigations so far show that transition to turbulence can be observed in

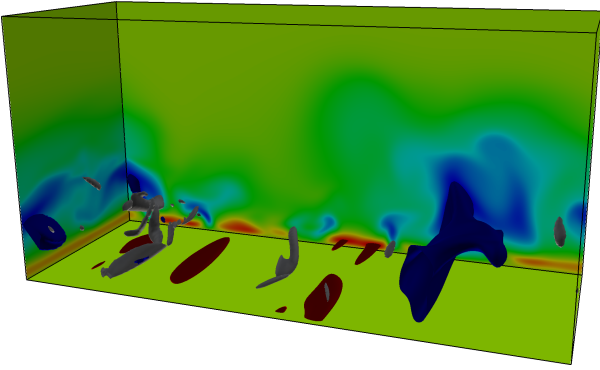


Figure 3: Three-dimensional visualisation of turbulent ASBL for $Re = 270$ in a numerical domain with $L_x = 6\pi$. Blue (low-speed streak) and red (high-speed streak) are the isosurfaces of streamwise velocity fluctuations $u' = -0.4$ and $u' = 0.2$. Vortices are visualised using the λ_2 criterion [35] with the isosurface $\lambda_2 = -0.01$. Flow from lower left to upper right.

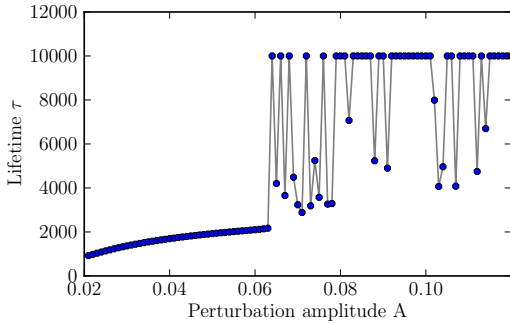


Figure 4: Lifetimes associated to trajectories starting from the initial condition \mathbf{u}_A , vs. the disturbance amplitude A , at $Re = 270$. $A = 1$ corresponds to the snapshot shown in fig. 3. The maximum observation time is here 10,000 time units.

the ASBL at least for $Re \gtrsim 250$ provided that the computational domain is large enough. Fig. 3 shows a typical turbulent state at $Re = 270$ and for $L_x = 6\pi$. A slightly higher computational domain with $L_y = 25$ was used in order to account for the thickening of the boundary layer typical for the turbulent ASBL [34]. The flow features clear coherent structures close to the wall in the form of high-speed streaks (shown in red) very near the lower wall, and low-speed streaks (blue) further up into the flow. The flow shows however no sign of spanwise localisation. The redistribution of momentum in the vertical direction is mainly due to the advection by streamwise vortices.

The turbulent regime in the chosen computational domain at such low values of Re is actually only metastable and the flow can rapidly relaminarise after a (sometimes extremely long) finite time. An investigation of lifetimes was performed at $Re = 270$ by considering the perturbation \mathbf{u}' to the laminar state \mathbf{U} displayed in fig. 3, rescaling its amplitude by a factor A , considering new initial conditions $\mathbf{u}_A(t = 0) = \mathbf{U} + A\mathbf{u}'$ and finally measuring the

lifetime of the turbulent regime as a function of A . Below a given threshold in A , all trajectories decay rapidly to the laminar state. Above this threshold $A \approx 0.06$ lifetimes increase dramatically and show huge fluctuations, with isolated initial conditions persisting forever. However, averaged over smooth sets of initial conditions, the mean lifetimes remain finite, indicating that the edge has been crossed [25]. In fig. 4 the lifetimes are displayed as a function of A showing a very fractal landscape. This situation, analogous to most subcritical shear flows at low enough values of Re , suggests the existence of a chaotic saddle [36]. As recently shown for the case of pipe flow and plane Couette flow [19, 20, 21], the creation of this chaotic saddle is due to a boundary crisis as Re is increased. This example of global bifurcation is typical in dynamical systems [37] and emerges when an already existing chaotic attractor collides with its basin boundary, which is the stable manifold of the edge state. In all studies of shear flows, the chaotic attractor preceding the boundary crisis emerges from a sequence of local bifurcations from an “upper branch” state originating from a saddle–node bifurcation. The other (unstable) state originating from that saddle–node is precisely the edge state. In practice, the studies in refs. [20, 21] all started with the identification of the edge state on the basin boundary, followed using continuation techniques down to the saddle–node bifurcation, where both lower and upper branches are created. This points out the importance of the edge state as the backbone of the turbulent dynamics, not only of the basin boundary. For larger values of Re , lifetimes tend to increase on average. Whether the turbulent regime remains transient or not at larger values of Re is beyond the scope of this study, however the concept of edge state remains robust. Note that the numerical continuation performed in former studies demands for technical reasons an edge state with trivial time dependence. In the remainder of the paper we investigate edge states in spanwise-extended ASBL and their dynamics.

3.2 Periodic edge states for $L_x = 6\pi$

From here on, the Reynolds number is held fixed at $Re = 500$. The edge state in the numerical domain of size

$(L_x, L_y, L_z) = (6\pi, 15, 50)$ has been discussed in detail in ref. [27], and we briefly summarise the main findings here. In this set-up three distinct edge states were found (modulo translational symmetries in x and z), two of which are related by the symmetry $z \rightarrow -z$. They all are localised in the spanwise direction and their dynamics is exactly periodic in time. The time evolution of the cross-flow energy E_{cf} for the states is shown in figs. 5(a) and 6(a). This quantity can be considered a measure for the amplitude of streamwise vortices and is defined as:

$$E_{cf} = \frac{1}{L_x L_z} \int_{\Omega} (v'^2 + w'^2) dx dy dz, \quad (6)$$

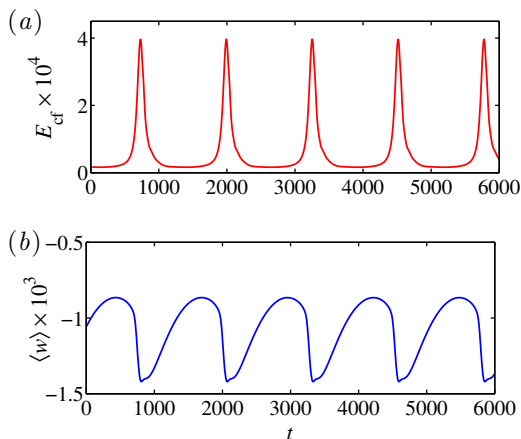


Figure 5: Time series for the left-shifting state (L) at $L_x = 6\pi$: (a) cross-flow energy E_{cf} ; (b) mean spanwise velocity $\langle w \rangle$.

where v' and w' are the wall-normal and spanwise velocity perturbations to the laminar solution (U, V, W) and Ω stands for the computational domain. For all three states the time signal alternates between calm regions with relatively low energy and bursts where significantly higher values in energy are realised. The temporal dynamics as well as the spatial structure of the edge states is shown in fig. 7 using a space–time diagram for the streamwise velocity perturbations u' evaluated at $y = 1$ and averaged in the x direction. During the calm phase the states consist of a pair of active high- and low-speed streaks with a slowly decaying low-speed streak on the side. After the burst of the cross-flow energy the structure is destroyed but rapidly reforms modulo a shift in the spanwise direction. Based on the direction of the translation we distinguish between the state alternatively shifting left and right (LR), and the ones shifting constantly in one direction, left (L, $z < 0$) or right (R, $z > 0$). The information about the translation direction can be extracted from the time series of the spatially-averaged spanwise velocity $\langle w \rangle = \int_0^{L_y} \hat{w}_{(0,0)} dy$ displayed in figs. 5(b) and 6(b), where $\hat{w}_{(0,0)}$ is the $(0, 0)$ mode of the Fourier discretisation in the horizontal plane at a given y position. Here $\langle w \rangle$ serves as a linear observable. Positive and negative values of $\langle w \rangle$ near the cross-flow energy peaks indicate shifts to the right and left, respectively.

The dynamics during one period of the cycle is similar for all three states, being equivalent to the one in the small domain [31], and bears strong resemblance with the self-sustaining cycle of wall turbulence described in ref. [38]. In the beginning of the calm phase the state consists of almost streamwise-independent streamwise streaks, with one of the low-speed streaks accompanied by a pair of quasi-streamwise vortices. The vortices increase in strength and size, further bending the streak (see fig. 8). Eventually the low-speed streak breaks up, which corresponds to the burst in the cross-flow energy.

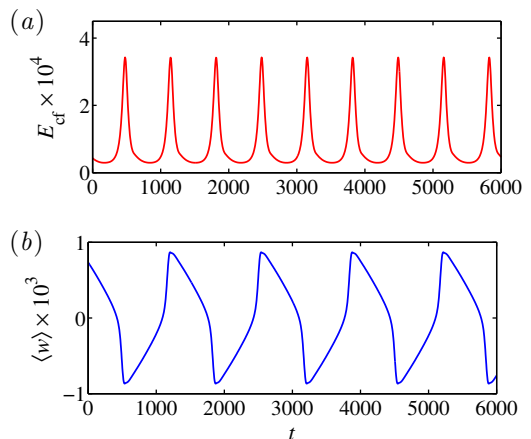


Figure 6: Time series for the left-right shifting state (LR) at $L_x = 6\pi$: (a) cross-flow energy E_{cf} ; (b) mean spanwise velocity $\langle w \rangle$.

During the breakdown process streamwise vortices are recreated in the vicinity of the destroyed low-speed streak. They lead to the creation of a high-speed streak at the same spanwise position with two low-speed streaks on the sides, and the loop is closed (see also ref. [27]). Thus, compared to the cycle from [38] there is an additional spatial aspect, manifesting itself in shifts of the structure in the spanwise direction.

The linear stability of the edge states with respect to perturbations within the basin boundary can be checked by considering return maps of $|\langle w \rangle|$ sampled at times corresponding to the maxima of E_{cf} . In such a representation a period- k orbit corresponds to k different points on the diagonal of the k -th return map. The slope β near these points in the return map should be equal and indicates the linear stability properties of the orbit: $|\beta| > 1$ indicates instability whereas $|\beta| < 1$ indicates stability. From fig. 9, which includes the approach to the L state in the first return map, we can for instance deduce that $\beta \approx 0.5$ and that the periodic orbit is hence a stable attractor on the edge.

3.3 Bifurcation diagram

When the length L_x of the computational domain is reduced to 4π , only few edge trajectories converge to a periodic LR state while the others stay erratic even for very long edge tracking times. In particular, we never got convergence to a periodic state when initiating the bisection with random initial conditions. Despite being erratic the state remains strongly localised in z for all times, with the active part consisting of a pair of low- and high-speed streaks. As in the periodic case, high- E_{cf} bursts are followed by spanwise translations of the whole structure. However, the time between the bursts is not constant and the shifts vary unpredictably in direction and distance. Understanding and characterising the bifurca-

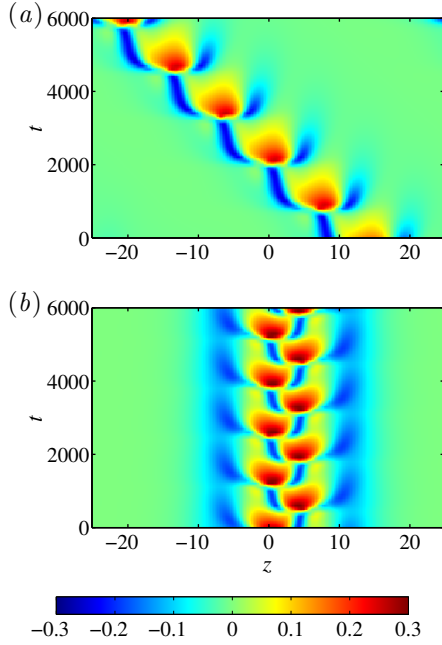


Figure 7: Space-time diagrams of the streamwise velocity fluctuations u' averaged in x at $y = 1$ for (a) the state shifting left (L) and (b) the state shifting repeatedly left and right (LR). For the online version: from blue to red, negative (low-speed streaks) to positive (high-speed streaks) values of u' .

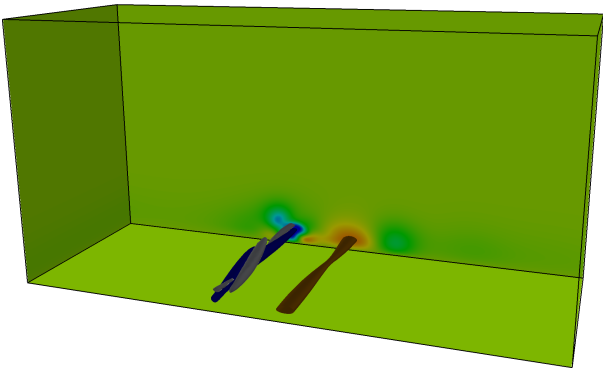


Figure 8: Snapshot of the L state for $L_x = 6\pi$ shortly before a burst. Isocontours are $u' = -0.2$ in blue, $u' = 0.1$ in red and $\lambda_2 = -0.001$ in grey. A pair of counter-rotating vortices can be identified leaning over the low-speed streak. On the right, a high-speed streak can be seen, the remnant of the preceding burst. Flow from lower left to upper right.

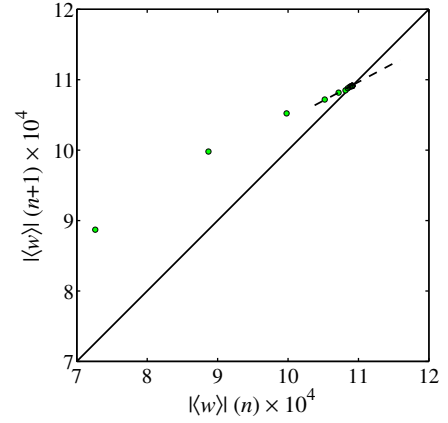


Figure 9: First return map of the absolute value of mean spanwise velocity $|\langle w \rangle|$ at the peaks of the cross-flow energy E_{cf} for the L state at $L_x = 6\pi$. The slope β of the approach to the diagonal, indicated by the dashed and solid lines, respectively, is close to 0.5, meaning that the state is stable.

tions connecting the periodic to the erratic regime is the focus of this study.

The long temporal period of the obtained states together with the large number of degrees of freedom involved, makes numerical continuation not feasible with the tools at hand. Therefore, we chose to vary the parameter L_x in discrete steps, starting from $L_x = 6\pi$. Since L and R states are the same under $z \rightarrow -z$ transformation, it is sufficient to focus on one of them only. Starting from $L_x = 6\pi$ the instantaneous flow fields of both L and LR states were shrunk to shorter domains. The resulting fields were used as initial conditions for the edge tracking, which was performed until the edge state in the considered domain was found. Initially, L_x was decreased from 6π to 4π in steps of 0.2π . As soon as qualitative changes were observed at some length, the same procedure was performed from the last periodic state with smaller step size. Decreases in L_x were regularly complemented with increases in L_x in order to check for hysteresis. Finally the important bifurcation regions were re-sampled using a finer resolution of 0.05π in L_x . The simulations altogether represent a total of nearly 10^6 CPU hours.

The results obtained using this procedure are displayed in fig. 10 via two bifurcation diagrams. In fig. 10(a), the maxima of E_{cf} are plotted for each value of L_x . We obtain two independent branches associated with L (squares) and LR (circles) states. Stable periodic states are represented by large filled symbols. If the state is n -periodic it corresponds to n different points in the diagram. Erratic states are denoted with smaller symbols. Unequal amount of points in different cases is due to varying length of the trajectories on the edge and irregular periods between two consecutive E_{cf} peaks. Nonetheless, each of the erratic simulations is an order of magnitude longer than the average time it takes to reach a periodic state, with

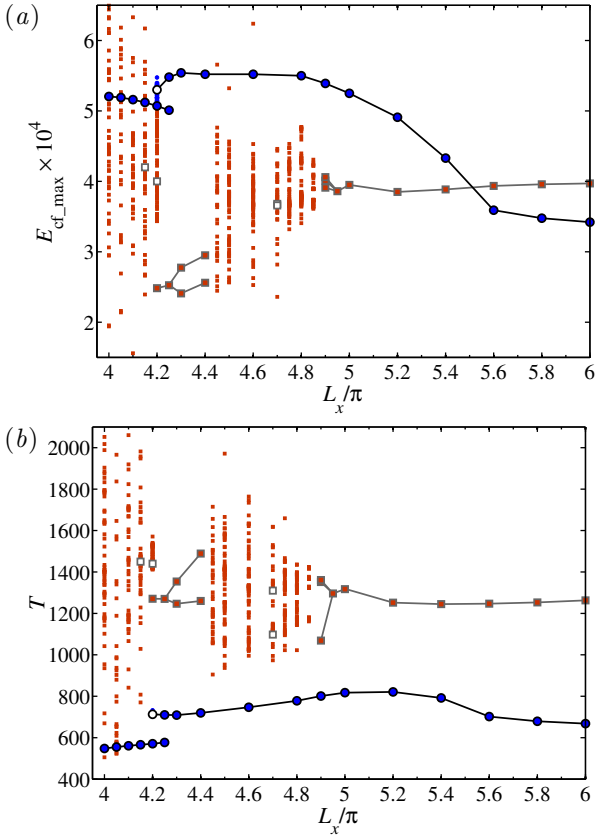


Figure 10: Bifurcation diagram in terms of (a) cross-flow energy peaks E_{cf_max} and (b) inter-burst periods T . The branches for the L and LR states are represented with squares (red online) and circles (blue online), respectively. Larger symbols represent stable (filled) and unstable (empty) states, whereas erratic behaviour is denoted with smaller symbols.

up to 100,000 time units in the longest chaotic simulations. If some range of values are frequently visited by the chaotic trajectory the corresponding state in the diagram is marked with a large empty symbol. In fig. 10(b) an alternative representation is shown, where the time intervals T between consecutive peaks of E_{cf} are considered instead. Some of the states identified within the bifurcation diagram are displayed in phase-space projections ($u_{rms}, v_{rms}, \langle w \rangle$), see fig. 11. The intervals in L_x chosen there contain the parameters where the aperiodic orbits are calculated and indicate how the orbits move with L_x . The aperiodic trajectories meander through phase space, transiently approach the loci of the L and R states associated to larger values of L_x and move between them along segments of the LR trajectory.

While the modulation in cross-flow energy of the LR state changes with L_x , the orbit stays exactly periodic until $L_x = 4.25\pi$. At $L_x = 4.2\pi$ it becomes weakly unstable, and the trajectory spends considerable time in its vicinity before leaving and exploring different part of the phase space. For some initial conditions, the localised

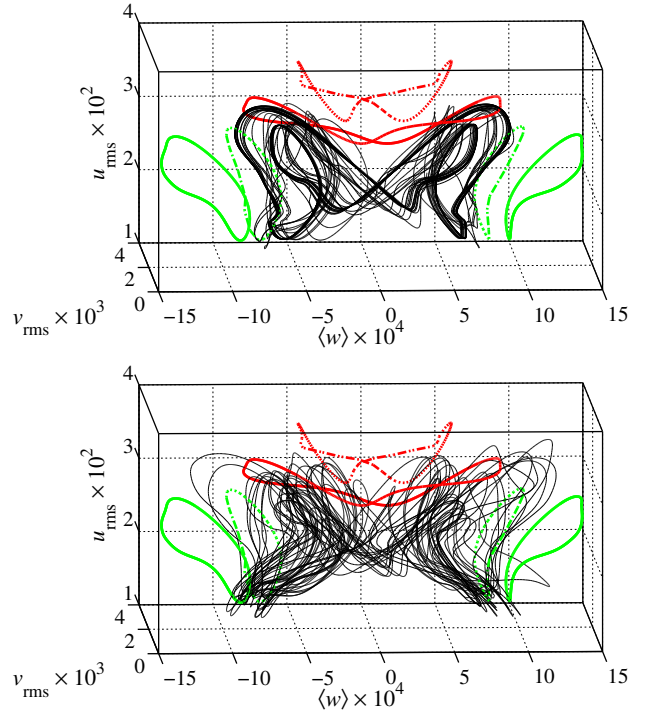


Figure 11: Representation of the dynamics in a space spanned by the mean spanwise velocity $\langle w \rangle$ and the root-mean-square velocity fluctuations in the wall-normal (v_{rms}) and streamwise (u_{rms}) components for length $L_x = 4.7\pi$ and $L_x = 4.5\pi$ in (a) and (b), respectively. The dynamics on the relative attractor within the edge (shown as a full line —) is intermittent in case (a) and erratic in case (b). In addition, we show the trajectories of the periodic LR state at $L_x = 6\pi$ (—) and $L_x = 4.6\pi$ (---), as well as that of the L and R states at $L_x = 6\pi$ (—) and $L_x = 5\pi$ (- - -).

state begins drifting in one direction (as described in the next paragraph). Some initial conditions lead to a new branch of LR states, characterised by a shorter period T . This new LR-branch has been tracked down to as low as $L_x = 3.6\pi$, below which periodicity in time is lost. It can also be continued to higher values of $L_x \geq 4.25\pi$, however we did not track the branch further. Whether it reconnects with the original LR branch remains an open question. This new state was not identified in ref. [27], which suggests that it has a smaller basin of attraction than the original LR state.

The stability range for the L state is narrower compared to the LR state, as it does not extend below $L_x = 4.95\pi$. For the next value we probed, $L_x = 4.9\pi$, a longer but stable 3-period state emerges as relative attractor on the edge, the full period of which consists of three consecutive shifts in each direction. We denote it by L^3R^3 (note that in fig. 10 two of the three symbols are very close to each other). Between 4.85π and 4.75π the dynamics is erratic in terms of the time evolution of the cross-flow energy, however repeating the same pattern of translations

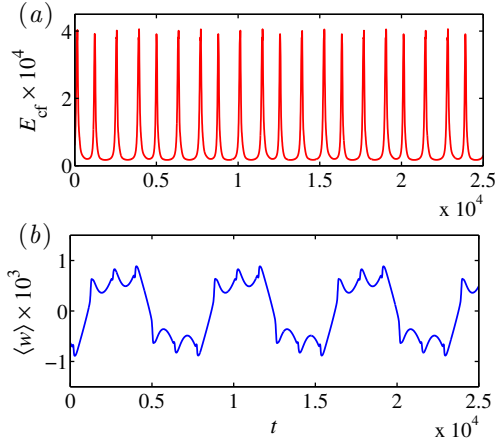


Figure 12: Time series for the 3-periodic L^3R^3 state at $L_x = 4.9\pi$: (a) cross-flow energy E_{cf} ; (b) mean spanwise velocity $\langle w \rangle$.

in the spanwise direction, with four consecutive shifts in each direction for $L_x = 4.85\pi$, three consecutive shifts in each direction for $L_x = 4.8\pi$ and irregular combinations between two and three shifts in each direction for $L_x = 4.75\pi$. The corresponding trajectories show no indication of convergence. Thus, even if the underlying orbits are stable, considerably longer simulation times may be required for convergence in this case. For $L_x = 4.7\pi$ Pomeau–Manneville intermittency is observed in the form of chaotic dynamics alternating with visits to an unstable L^2R^2 orbit. Below this value the dynamics is erratic, except in a stable period-1 and a period-2 window between 4.2π and 4.4π , where an L state is recovered again. Additionally, an intermittently chaotic L state is obtained from the LR-branch at 4.2π and on the L-branch at 4.15π . It is marked with empty squares for the corresponding values of L_x in the bifurcation diagram. Due to the interesting dynamics on this branch, some parameter values will be discussed in more detail below.

3.4 Investigation of the L-branch

3.4.1 Period-3 state ($L_x = 4.9\pi$)

For $L_x = 4.9\pi$ a longer periodic state is obtained. As is evident from fig. 12, the state is 3-periodic in terms of the time evolution of E_{cf} . Part of the space–time diagram for this state is shown in fig. 13(a), where the state is seen to alternate between three shifts in each direction. We thus denote this state as L^3R^3 .

3.4.2 Intermittent state ($L_x = 4.7\pi$)

Lowering L_x down to 4.7π on the L-branch, the periodic behaviour is lost. Part of the time evolution of E_{cf} and $\langle w \rangle$ in this case is shown in fig. 14. The dynamics seems to repeatedly spend considerable amount of time

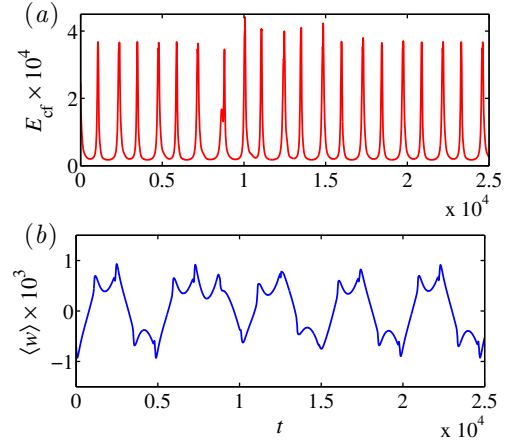


Figure 14: Time series for the intermittent state at $L_x = 4.7\pi$: (a) cross-flow energy E_{cf} ; (b) mean spanwise velocity $\langle w \rangle$.

in the vicinity of the state with two shifts in each direction (L^2R^2), before suddenly leaving and being quickly re-injected again. These transient approaches to the L^2R^2 state can be clearly seen in fig. 15, where the maxima of the cross-flow energy E_{cf_max} are plotted against time for the full trajectory. Again, in order to assess the stability of this 2-period state the second return map of $|\langle w \rangle|$ is considered (see fig. 16). Clearly, both slopes near the diagonal are larger than 1, meaning that the underlying L^2R^2 state exists at least for neighbouring parameters and is here not stable. A part of the space–time diagram capturing this phenomena is shown in fig. 13(b), where regular L^2R^2 shifts are interrupted by short aperiodic motion. A phase-space representation of this state, together with some of the periodic states is shown in fig. 11(a). Despite the chaotic motion, the underlying structure of the L^2R^2 orbit can be identified.

This type of behaviour was first described by Pomeau and Manneville in 1980 as a key element of transition to chaos through intermittency [39]. Depending on the bifurcation leading from periodic to intermittent dynamics different types of intermittency are defined. In practice, in order to identify the relevant intermittency scenario, converged statistics of the inter-burst times would be needed for a continuous range of values L_x close to the bifurcation point, which is too costly.

3.4.3 Chaotic state ($L_x = 4.5\pi$)

Reducing L_x further, no periodic states are identified on the L-branch between $L_x = 4.6\pi$ and $L_x = 4.45\pi$. The time signal of the cross-flow energy, shown in fig. 17 for $L_x = 4.5\pi$, is erratic, while still experiencing calm and bursting phases. As can be seen from the space–time diagram in fig. 13(c), the state does not change structurally, keeping the same characteristic lengthscales and timescales. However its spatio-temporal dynamics is no

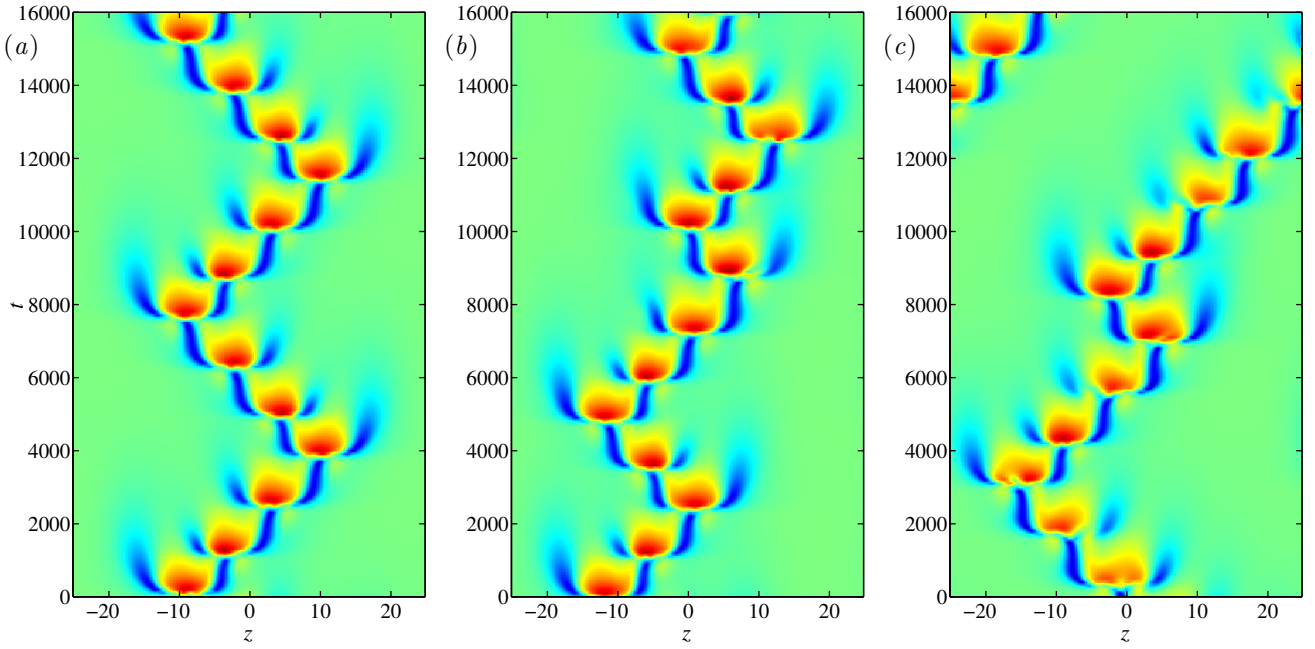


Figure 13: Space–time diagrams of the streamwise velocity fluctuations u' averaged in x at $y = 1$ for some states on the L-branch: (a) Period-3 state at $L_x = 4.9\pi$ (L^3R^3); (b) Intermittent state at $L_x = 4.7\pi$; (c) Chaotic state at $L_x = 4.5\pi$. The colourmap is the same as in fig. 7.

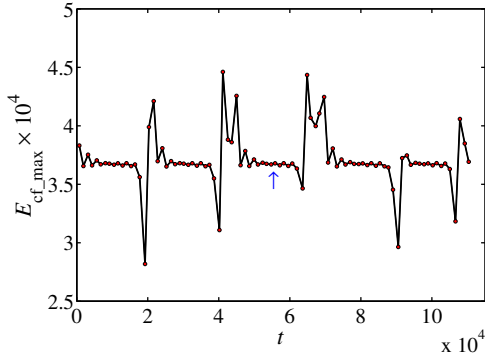


Figure 15: Cross-flow energy maxima $E_{cf,max}$ for the intermittent state at $L_x = 4.7\pi$. The starting time for fig. 13(b) and fig. 14 corresponds to $t = 54,800$ in this representation, marked with the vertical arrow in the figure.

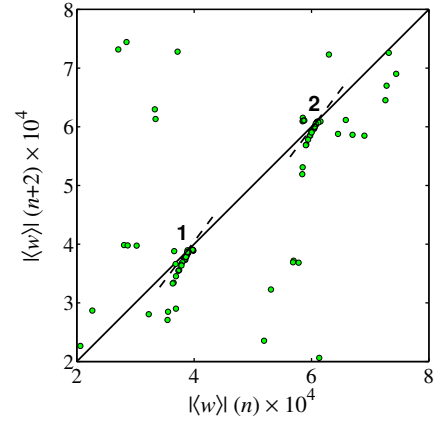


Figure 16: Second return map of $|\langle w \rangle|$ at the peaks of E_{cf} for the intermittent state at 4.7π . Both slopes, indicated by the dashed lines, are approximately the same and are larger than 1, with $\beta_1 \approx \beta_2 \approx 1.3$, proving that the L^2R^2 orbit is unstable on the edge.

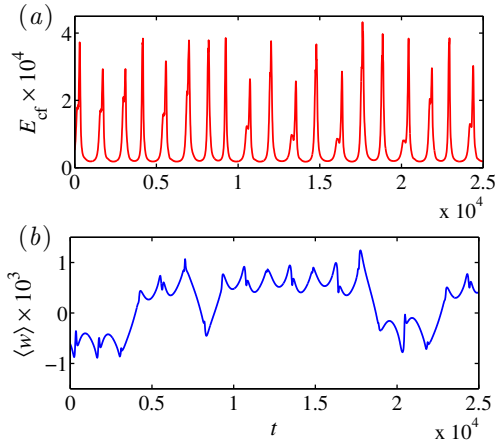


Figure 17: Time series for the erratic state at $L_x = 4.5\pi$: (a) cross-flow energy E_{cf} ; (b) mean spanwise velocity $\langle w \rangle$.

longer regular but features a random walk, with unpredictable spanwise shifts occurring at non-regular times. The various return maps did not reveal any clear structure and we refer to this state as "chaotic" or "erratic". A phase-space representation of such a state is displayed in fig. 11(b).

3.4.4 Period doubling ($L_x = 4.3\pi$)

Below $L_x = 4.45\pi$ the state which repeatedly shifts only in one direction becomes attracting again. However unlike the previously identified L state, two consecutive translations are no longer equivalent (see fig. 18). The spatio-temporal dynamics consists of two shifts of different lengths in the same direction. Their duration is different by less than 20% and the total period of the state is approximately twice the period found for larger L_x . We thus denote this edge state by L^2 and call somewhat abusively "period-doubled". Somewhere between $L_x = 4.3\pi$ and $L_x = 4.25$ the state undergoes a reverse period doubling bifurcation, and the original L state is recovered. It is stable down to $L_x = 4.2\pi$, below which the dynamics becomes chaotic again. Notable intermittent approaches to another periodic state were identified for $L_x = 4.15\pi$, as well as for $L_x = 4.2\pi$ for other non-converging edge trajectories.

3.5 Transition to turbulence from the edge states

Once the edge state is reached, simulations with initial conditions slightly above the separatrix produce trajectories which stay for a finite time in the vicinity of the edge state and then rapidly leave towards the turbulent state along the leading unstable direction. Since the time scales of escape to turbulence are smaller than the scales of periodic motion that defines the states, the overall features of the transition process are similar when starting from different states. Space-time diagrams depicting departure

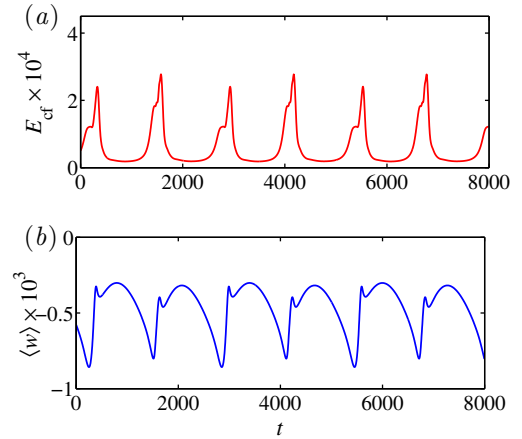


Figure 18: Time series for the 2-periodic L^2 state at $L_x = 4.3\pi$: (a) cross-flow energy E_{cf} ; (b) mean spanwise velocity $\langle w \rangle$.

from edge state to turbulence are shown in fig. 19. Once the evolution leaves the edge state the structure quickly delocalises in z and spreads over the full domain. This is independent of where exactly the deviation from the edge trajectory occurs first. As seen in fig. 20, close to the edge state, not only the active low-speed streak becomes turbulent, but also the one which decays when confined to the edge develops sinuous instabilities. In contrast to Couette flow [18] where the generated streaks have been found to be stationary in space, in the present ASBL case the low- and high-speed streaks in the spreading turbulence are also drifting in the spanwise direction. Nucleation of new streaks appears to be reminiscent of the spanwise translations of the discussed edge states.

4 Discussion, perspectives

When confined to the laminar-turbulent separatrix, the present system exhibits complex dynamics, with coexistence of more than one attractor. The complexity raises questions about how those attracting states are connected together. They can either belong to different families of solutions or be connected through local bifurcations. Multistability is typical in low-dimensional systems (see ref. [40] and related references) and can be also found in hydrodynamical settings (see *e.g.* ref. [41]). For some values of the parameter L_x we identified here an unusual competition between a periodic and an erratic state. Performing edge state tracking in this situation, very long simulation times can be needed to decide whether the algorithm has converged to a chaotic state or is still converging to a simpler state. This demonstrates the limitations of the edge tracking procedure for understanding and characterising the full structure of the laminar-turbulent boundary using a finite (small) number of simulations only. Conversely,

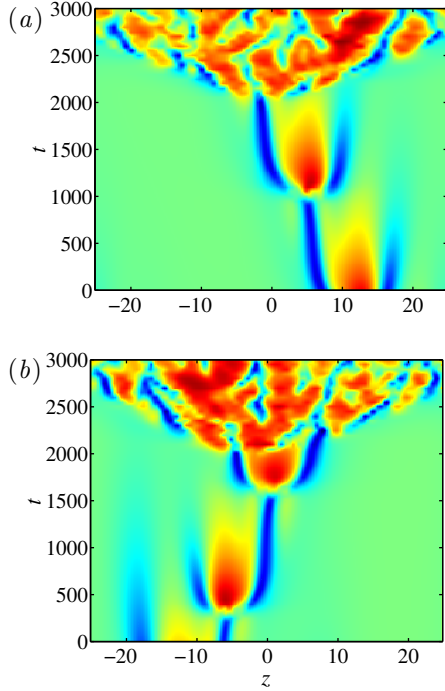


Figure 19: Space–time diagrams of the streamwise velocity fluctuations u' averaged in x at $y = 1$ showing transition to turbulence from (a) L state at $L_x = 6\pi$; (b) Intermittent state at $L_x = 4.7\pi$. The colourmap is the same as in fig. 7.

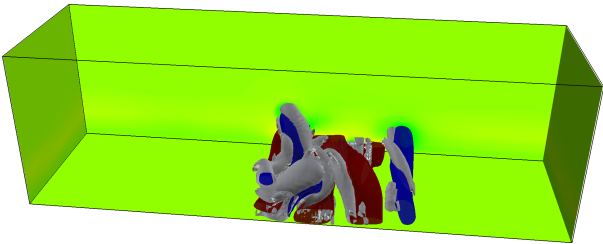


Figure 20: Snapshot on the trajectory going turbulent of the L^2R^2 state for $L_x = 4.7\pi$ at $t = 2,000$ in fig. 19(b). Isocontours are $u' = -0.2$ in blue, $u' = 0.1$ in red and $\lambda_2 = -0.001$ in grey. The active left low-speed streak has already gone turbulent, whereas the right low-speed streak, which would decay when confined to the edge, also develops sinuous instabilities. Flow from lower left to upper right.

the linear stability properties of an edge state give no indication about the size of its basin of attraction, the latter being a fully nonlinear concept. In some situations this can lead to a misinterpretation of the dynamical role of some stable solutions, as pointed out in ref. [42] using a counterexample from a low-dimensional toy model.

Still, we were able to obtain a finer characterisation of the edge structure than, for instance, in ref. [26]. We suggest here a qualitative explanation of some exotic behaviours expected on the edge, such as multistability and intermittency. Our suggestion is based on compiling results on exact coherent structures from other subcritical shear flows, notably the influence of varying either the streamwise or spanwise wavelength of the numerical domain. The use of arc-length continuation robustly showed that most fundamental solutions such as travelling waves or steady states are born and destroyed in saddle–node bifurcations [43, 44, 45]. Among these solutions, those with only one unstable eigendirection should in principle correspond to edge states. The coexistence of several loops of solutions in parameter space is typical and thus multistability should be found on the edge when several solutions with only one unstable multiplier overlap in a given range of parameters. Such a situation has already been reported in ref. [26] for the travelling waves in pipe flow with $m = 2$ symmetry. In the vicinity of these saddle–node bifurcations, type-I intermittency [39] should be found. In the present study we deal with spanwise-localised solutions, hence the width of the domain L_z is irrelevant once large enough. However we do report multistability in some windows of the parameter L_x and intermittency for other values of L_x .

The above scenario is summarised graphically in fig. 21. We suppose (by direct analogy with former studies) that periodic solutions such as those identified for $L_x = 6\pi$ emerge as loops in fig. 21(a). The y -axis refers to a suitable scalar observable, for instance $E_{cf,max}$ (used in fig. 10(a)) or v_{rms} , the quantity used to iteratively find edge states. Knowledge of the stability properties of each branch (including possible local bifurcations along these branches) allows to list the solutions potentially behaving locally as relative attractors on the edge. Locating the saddle–node bifurcations associated precisely with these solutions also allows for predicting regions in L_x where intermittency can be expected on the edge. This is shown in fig. 21(b), which is graphically deduced from fig. 21(a) and compares conceptually well with the numerical bifurcation diagram of fig. 10(a).

It is noteworthy that multistability and intermittency are not observed if the width of the domain L_z is small. In ref. [31] edge states which are periodic in both wall-parallel directions are studied and the range in L_x that we investigated here is also covered. However, only one edge state is found; it is only the spanwise localisation

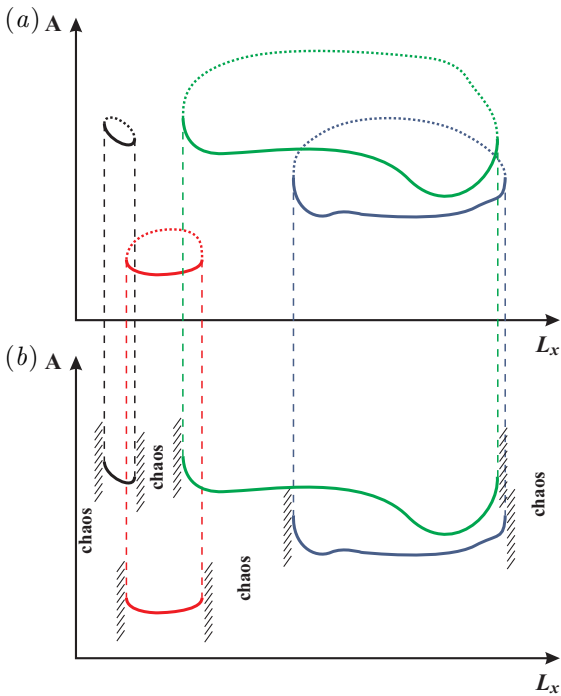


Figure 21: Conceptual sketch of (a) exactly periodic solutions as a function of L_x and (b) the corresponding bifurcation diagram for the dynamics on the edge. Solid lines represent solutions with one unstable direction, whereas dashed lines – with more than one. The thin vertical dashed lines connect the saddle–node bifurcation points between the upper and the lower part of the figure. Hatched areas indicate possible intermittency zones.

that allows multiple states to coexist in the same domain.

We note, as many authors before us, that the total number of unstable directions of solutions lying on the edge is necessarily low, being equal to 1 for edge states and finite otherwise. For the parameter values where edge trajectories stay erratic, consisting of transient approaches to finite-amplitude solutions with at least 2 unstable eigenvalues, the number of unstable Lyapunov exponents must also remain small. Moreover, the robust spatial localisation of these edge states, verified in ref. [27], implies that increasing the domain size in the direction of localisation does not modify the dynamics, and hence does not change the number of unstable Lyapunov exponents even in chaotic regimes. The dynamics on the edge, though genuinely spatio–temporal, can hence safely be interpreted as an example of non-extensive and low-dimensional dynamics. This has to be contrasted with the associated turbulent regime existing for the same parameters. The turbulent regime is not spatially localised and thus represents extensive chaos. Quantitative estimation of the number of unstable Lyapunov exponents of typical turbulent trajectories is a hard task. A numerical estimate of this number was given in ref. [46] in the case of a “minimal” turbulent

channel flow at $Re_\tau = 180$, and was found to be 352, *i.e.* very large. Though analogies between all these different flows are to be taken cautiously, the different orders of magnitude are unambiguous. The dynamics on the edge features a very small number of unstable dimensions while the dynamics in the turbulent regime is highly unstable. This strongly supports the investigation of edge states as a laboratory for investigating the dynamics and the self-sustenance mechanisms of coherent structures arising in turbulent flows.

We have here identified and characterised several edge states in spanwise-extended ASBL for different streamwise wavelengths. All these states are structurally the same, consisting of an active localised pair of low- and high-speed streaks with streamwise vortices. The dynamics of the streaks is built on the same elements as in the simplest L/LR cycles, *i.e.* bursts and spanwise shifts, regardless of the nature of the regime. Very similar coherent structures and dynamics were also found to be the minimal self-sustaining elements of near-wall turbulence [47, 38, 48, 49, 28]. Moreover, comparing the three-dimensional visualisations of both turbulence and the edge state in figs. 3 and 8, similarities are obvious, let alone the localisation properties, and closer comparison deserves more intensive investigation.

While edge states were first identified in small periodic domains, they have localised counterparts when the domain is extended in at least one planar direction. The dynamics of such solutions usually mimics the one found in smaller domains (*e.g.* bursts in cross-flow energy in the case of ASBL). These localised solutions emerge from the spatially periodic branches either through a snaking scenario [17] or through large wavelength instabilities [50, 51, 52]. The study in ref. [52] showed that streamwise-localised relative periodic orbits bifurcate off streamwise-periodic travelling waves in pipe flow. By analogy we can thus expect that new fully localised solutions in ASBL bifurcate off the time-periodic spanwise-localised solutions presented here.

In summary we have studied the dynamics on the laminar–turbulent separatrix for a boundary-layer flow in a spanwise-extended set-up with varying streamwise periodicity. We were able to find a multitude of periodic and erratic edge states, which all share the same structure. The bifurcation diagram obtained by compiling all these results contains a variety of interesting phenomena whose study is usually restricted to the framework of low-dimensional ODEs or iterated maps. Those include multistability, intermittency and period doubling. Besides their properties as examples of simple dynamics embedded in a high-dimensional space, the identified states also constitute an interesting prototype flow for understanding the self-sustaining mechanism of near-wall turbulence and developing nonlinear control strategies.

Acknowledgements

T. Kh. would like to thank Paul Manneville and Predrag Cvitanović for discussions about the bifurcation diagram. Computer time provided by SNIC (Swedish National Infrastructure for Computing) is gratefully acknowledged.

References

- [1] P.J. Schmid, D.S. Henningson, *Stability and Transition in Shear Flows* (Springer, New York, 2001)
- [2] T. Herbert, *Annu. Rev. Fluid Mech.* **20**, 487 (1988)
- [3] H. Schlichting, *Boundary-Layer Theory*, 7th edn. (McGraw-Hill, New York, 1987)
- [4] L.M. Hocking, *Q. J. Mech. Appl. Math.* **28**, 341 (1975)
- [5] O. Dauchot, P. Manneville, *J. Phys. II* **21**, 371 (1997)
- [6] P. Manneville, in *IUTAM Symposium on Laminar-Turbulent Transition and Finite Amplitude Solutions*, edited by T. Mullin, R. Kerswell (Springer Netherlands, 2005), Vol. 77 of *Fluid Mechanics and its Applications*, pp. 1–33
- [7] O. Levin, D.S. Henningson, *J. Fluid Mech.* **584**, 397 (2007)
- [8] B. Eckhardt, T.M. Schneider, B. Hof, J. Westerweel, *Annu. Rev. Fluid Mech.* **39**, 447 (2007)
- [9] J.D. Skufca, J.A. Yorke, B. Eckhardt, *Phys. Rev. Lett.* **96**, 174101 (2006)
- [10] G. Kawahara, *Phys. Fluids* **17**, 041702 (2005)
- [11] F. Mellibovsky, A. Meseguer, T.M. Schneider, B. Eckhardt, *Phys. Rev. Lett.* **103**, 054502 (2009)
- [12] Y. Duguet, P. Schlatter, D.S. Henningson, *Phys. Fluids* **21**, 111701 (2009)
- [13] T.M. Schneider, D. Marinc, B. Eckhardt, *J. Fluid Mech.* **646**, 441 (2010)
- [14] Y. Duguet, A.P. Willis, R.R. Kerswell, *J. Fluid Mech.* **663**, 180 (2010)
- [15] Y. Duguet, P. Schlatter, D.S. Henningson, B. Eckhardt, *Phys. Rev. Lett.* **108**, 044501 (2012)
- [16] E. Knobloch, *Nonlinearity* **21**, T45 (2008)
- [17] T.M. Schneider, J.F. Gibson, J. Burke, *Phys. Rev. Lett.* **104**, 104501 (2010)
- [18] Y. Duguet, O. Le Maître, P. Schlatter, *Phys. Rev. E* **84**, 066315 (2011)
- [19] F. Mellibovsky, B. Eckhardt, *J. Fluid Mech.* **709**, 149 (2012)
- [20] T. Kreilos, B. Eckhardt, *Chaos* **22**, 047505 (2012)
- [21] M. Avila, F. Mellibovsky, N. Rolland, B. Hof, *Phys. Rev. Lett.* **110**, 224502 (2013)
- [22] P. Manneville, *Phys. Rev. E* **79**, 025301 (2009)
- [23] K. Avila, D. Moxey, A.D. Lozar, M. Avila, D. Barkley, B. Hof, *Science* **333**, 192 (2011)
- [24] J. Vollmer, T.M. Schneider, B. Eckhardt, *New J. Phys.* **11**, 013040 (2009)
- [25] T.M. Schneider, B. Eckhardt, J.A. Yorke, *Phys. Rev. Lett.* **99**, 034502 (2007)
- [26] Y. Duguet, A.P. Willis, R.R. Kerswell, *J. Fluid Mech.* **613**, 255 (2008)
- [27] T. Khapko, T. Kreilos, P. Schlatter, Y. Duguet, B. Eckhardt, D.S. Henningson, *J. Fluid Mech.* **717**, R6 (2013)
- [28] J. Jiménez, G. Kawahara, M.P. Simens, M. Nagata, M. Shiba, *Phys. Fluids* **17**, 015105 (2005)
- [29] S. Cherubini, P. De Palma, J.C. Robinet, A. Bottaro, *Phys. Fluids* **23**, 051705 (2011)
- [30] D. Biau, *Phys. Fluids* **24**, 034107 (2012)
- [31] T. Kreilos, G. Veble, T.M. Schneider, B. Eckhardt, *J. Fluid Mech.* **726**, 100 (2013)
- [32] A.P. Kuznetsov, S.P. Kuznetsov, I.R. Sataev, *Int. J. Bifurcat. Chaos* **3**, 139 (1993)
- [33] M. Chevalier, P. Schlatter, A. Lundbladh, D.S. Henningson, *Tech. Rep. TRITA-MEK 2007:07*, KTH Mechanics, Stockholm, Sweden (2007)
- [34] P. Schlatter, R. Örlü, *Turbulent asymptotic suction boundary layers studied by simulation*, in *Journal of Physics: Conference Series* (IOP Publishing, 2011), Vol. 318, p. 022020
- [35] J. Jeong, F. Hussain, *J. Fluid Mech.* **285**, 69 (1995)
- [36] A. Schmiegell, B. Eckhardt, *Phys. Rev. Lett.* **79**, 5250 (1997)
- [37] K.T. Alligood, T.D. Sauer, J.A. Yorke, *Chaos* (Springer, New York, 1996)
- [38] J.M. Hamilton, J. Kim, F. Waleffe, *J. Fluid Mech.* **287**, 317 (1995)
- [39] Y. Pomeau, P. Manneville, *Commun. Math. Phys.* **74**, 189 (1980)
- [40] A.N. Pisarchik, C. Grebogi, *Int. J. Bifurcat. Chaos* **18**, 1605 (2008)
- [41] F. Feudel, N. Seehafer, L.S. Tuckerman, M. Gellert, *Phys. Rev. E* **87**, 023021 (2013)
- [42] N. Lebovitz, *Nonlinearity* **22**, 2645 (2009)
- [43] H. Faisst, B. Eckhardt, *Phys. Rev. Lett.* **91**, 224502 (2003)
- [44] H. Wedin, R.R. Kerswell, *J. Fluid Mech.* **508**, 333 (2004)
- [45] J.F. Gibson, J. Halcrow, P. Cvitanović, *J. Fluid Mech.* **638**, 243 (2009)

- [46] L. Keefe, P. Moin, J. Kim, *J. Fluid Mech.* **242**, 1 (1992)
- [47] J. Jiménez, P. Moin, *J. Fluid Mech.* **225**, 213 (1991)
- [48] W. Schoppa, F. Hussain, *J. Fluid Mech.* **453**, 57 (2002)
- [49] S. Toh, T. Itano, *J. Fluid Mech.* **481**, 67 (2003)
- [50] K. Deguchi, P. Hall, A. Walton, *J. Fluid Mech.* **721**, 58 (2013)
- [51] K. Melnikov, T. Kreilos, B. Eckhardt (2013), unpublished
- [52] M. Chantry, A.P. Willis, R.R. Kerswell (2013), unpublished, [arXiv:1308.6224](https://arxiv.org/abs/1308.6224)